Nanoscale

Accepted Manuscript

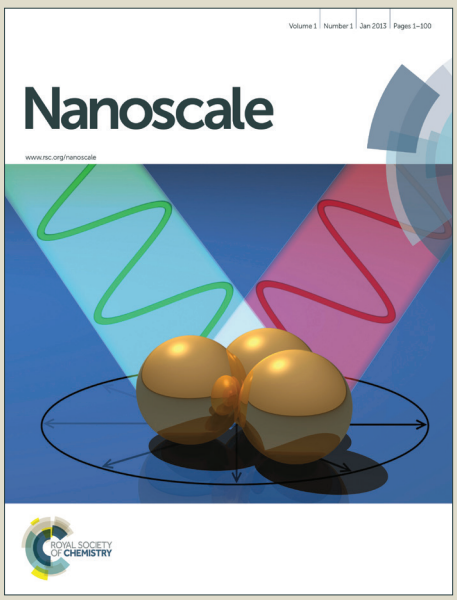

ROYAL SOCIETY OF CHEMISTRY

www.rsc.org/nanoscale

Designer Ge/Si composite quantum dots with enhanced thermoelectric properties

Hung-Tai Chang, Sih-Yuan Wang, and Sheng-Wei Lee*

Institute of Materials Science and Engineering, National Central University, Jhongli, 32001 Taiwan, Republic of China

Abstract

An otherwise random, self-assembly of Ge/Si composite quantum dots (CQDs) on Si has been controlled by the inserting layer of Si, sub-dot stacks, and post-annealing to produce micron-scale-thick QD layers with desired QD morphology, interface density, and composition distribution. A heterostructure consisting of a deliberate insertion of Si between Ge sub-dots is shown to improve the epitaxial coherence of the Ge QDs by the suppression of Ge surface interdiffusion and coarsening. Compared to the regular-QD materials, the thin-film-like multifold-CQD materials are found to exhibit both a reduced cross-plane thermal conductivity and an enhanced electrical conductivity, and a 1.5 times higher *ZT* value by calculation, providing a promising building block for practical thermoelectric applications in micro- or nanoelectronics.

*Corresponding author's name: Sheng-Wei Lee

Postal address: *Institute of Materials Science and Engineering, National Central University, No.300, Jhongda Rd., Jhongli City, Taoyuan County 32001, Taiwan*

Telephone number: 886-3-4227151 ext. 34905

Fax number: 886-3-2805034

E-mail address: swlee@ncu.edu.tw

1. Introduction

Recently high figure-of-merit (*ZT*) thermoelectric (TE) materials that efficiently convert heat into electricity or vice versa have attracted considerable attentions for providing one of promising solutions to sustainable energy technology.[1-5] For a high performance TE material, the concurrent of low thermal conductivity (κ) and high electrical conductivity (σ) is essential since *ZT* increases linearly with σ and is inversely proportional to κ.[6,7] However, to boost *ZT* of bulk TE materials is extremely challenging because of a strong interdependence of these key physical parameters that involve both charge transport properties and phonon transport behaviors. Generally, the optimization of one parameter adversely affects another. Encouragingly, nanostructuring TE materials that effectively reduces lattice conductivity in conjunction with no obvious influence on electrical properties, has been recognized as the most successful approach for significantly increasing the *ZT* value.[8-10] This is enabled by the fact that in the nano-scale or low-dimensional regime, the large difference in the mean free paths (MFPs) between electron and phonon provides an opportunity to decouple the phonon transport from charge transport.[11,12]

Many attempts have been made on the exploration of Si/Ge superlattices for TE applications. While planar Si/Ge superlattices exhibit very low cross-plane κ ($\kappa_{\perp}$), the large type-II band alignment in strained and relaxed SiGe heterostructures do not favor cross-plane carrier transport, making it difficult to reach enhanced ZT.[13] Another potential way to improve cross-plane carrier transport is through the use of Ge/Si quantum dot (QD) superlattice, in which arrays of Ge dots are separated from one another by thin Si spacers.[14,15] Over the past years, many efforts have been dedicated to the fabrication of Ge QD nanostructures, on which a significant reduction in κ was achieved due to enhanced phonon scattering.[16,17] The major challenge on the epitaxy of QD TE materials lies in the growth of sufficient amount or micrometer-scale QD films from TE conversion perspectives. It is of

extreme difficulty on the epitaxial growth of thin-film-like Ge QD materials using atomic layer deposition techniques arising from thermodynamic limitations on the structural parameters of QDs. A self-assembly of Ge QDs on Si is able to be created in the Stranski–Krastanow (SK) growth mode, however, the QD morphology varies with the QD volume that involves a transition from an initial pyramids (or transition pyramids), through square-based pyramids or rectangular-based huts, to the ultimate multifaceted domes in a sequence of volume evolution.[18,19] A further increase in the QD volume even results in the appearance of dislocated superdomes as a result of strain relaxation by dislocation injection . Also during the growth of thin-film-like SK QD materials, too thin a Si spacer or excessive Ge deposition is prone to the Ge QDs coarsening and the defect generation,[20,21] thus deteriorating the TE performance. Another challenge on TE materials is the accurate tailoring on TE properties of thin-film-like QD materials with high spatial resolution that is crucial for thermal management of nanoelectronics, or for nanoscale energy conversion. The tunable physical properties of QDs is determined by the precise control over QD structural parameters, such as dot size and composition that are interrelated.[22]

Recently, we demonstrated that a multifold Ge/Si/Ge composite QD (CQD) heterostructure is able to break through this fabrication bottleneck and effectively suppress the generation of dislocations in the thin-film-like materials.[23] In this study, we advance the growth of the CQD heterostructures to demonstrate that the structural parameters of CQDs, including dot size and morphology, Si/Ge interface density, and composition distribution in dots, are effectively tunable by the thickness of inserted Si as well as the stack number of the multifold CQDs, or through a post-growth annealing process. The distinct formation mechanism for a variety of CQDs is clarified by selective chemical etching experiments. More importantly, compared to the regular-QD materials, the thin-film-like CQD materials exhibit both reduced $\kappa_{\perp}$ and enhanced σ, leading to a potential higher ZT value. These results

show that such thin-film-like CQD materials are promising building blocks for TE applications in micro- or even nanoelectronics.

2. Experimental

All Ge-QD samples were grown at 600 ℃ in an ultra-high vacuum chemical vapor deposition (UHV/CVD) system. Pure SiH_4 and GeH_4 were used as gas precursors for Si and Ge deposition, respectively. The Si wafers were dipped in a diluted HF solution prior to deposition for creating a hydrogen-passivated surface. After the deposition of a 50-nm-thick buffer layer of Si, multifold Ge (12.6 ML)/Si (2 nm)/Ge (12.6 ML) heterostructures were deposited for the formation of self-assembled CQDs, in which the thickness of inserted Si and the number of Ge stacks were varied. The main difference in the structures between CQDs and regular QDs is the deliberate insertion of thin Si between Ge sub-dots for the CQDs. For simplicity, we refer the Ge/Si/Ge structure as 2-fold CQDs. Along the line with the incorporation of more Ge stacks into a CQD structure, 3- and 5-fold CQDs (Ge/Si/Ge/Si/Ge and Ge/Si/Ge/Si/Ge/Si/Ge, respectively) were produced. An *in-situ* annealing at the growth temperature for 1 h was conducted right after the CQDs growth to investigate the thermal stability and tunability of the structural parameters. For $\kappa_{\perp}$ and σ measurements, we produced a thin-film-like material of 40-period multifold CQDs stacks with a thickness as high as ~ 1.2 μm, in which the thickness of Si spacer layer between each CQD layer was fixed at 20 nm. Two sets of regular QDs formed by deposition of 12.6 and 25.2 ML Ge, respectively, were also prepared as reference samples for comparison.

Recently it has been shown that selective chemical etching combined with atomic force microscopy (AFM) can be utilized to obtain useful information about the composition of SiGe nanostructures. Based on the selectivity of a H_2O_2- or BPA-containing solution, that etches preferentially Ge over Si, it was possible to follow the time evolution of the etching process

and to determine the spatial distribution of Si and Ge in Ge QDs with a resolution of a few nanometers.[18,24-26] In this study, selective chemical etching was conducted on the CQD samples at room temperature to reveal their composition distributions as well as to study their formation mechanisms. A mixture of NH_4OH, H_2O_2, and deionized water was used as the etchant that selectively removes Ge over Si at room temperature and has an extremely low etching rate for the SiGe alloy with Ge composition less than 30%.[24] The surface morphologies of CQD samples before and after etching were characterized *ex situ* using AFM in tapping mode. To analyze the island facets in detail, surface orientation maps (SOMs) were further extracted. Transmission electron microscopy (TEM) characterization was performed to reveal detailed information about the microstructures of CQDs. For $\kappa_\perp$ characterization, the thin-film-like CQD samples were capped with a 50-nm-thick SiO_2 layer using inductively coupled plasma CVD followed by Al deposition and lift-off process to produce 200-μm-length, 4-μm-width, and 500-nm-thick Al heater lines. Variable-temperature measurements on $\kappa_\perp$ using the differential 3ω technique were performed in a high-vacuum cryostat (~10^{-6} torr) to prevent heat conductive or convective loss to the surrounding gaseous media. The thermal resistance contribution from a controlled sample of SiO_2/Si was measured separately as a subtraction reference for SiO_2/CQDs/Si samples. For σ characterization, the thin-film-like CQD samples were implanted with 70 keV B^+ ions at a dose of 5×10^{15} cm^{-2}. The dopants were activated at 900 ℃ for 3 min. Temperature- dependent σ was characterized using the four-probe technique.

3. Results and discussion

The AFM and cross-sectional TEM (XTEM) micrographs in Fig. 1 illustrate the necessity and influence of a thin separating layer of Si in CQDs in the presence of excess Ge deposition. Fig. 1(a) shows the surface morphology of as-grown regular QDs that were

produced by an excessive deposition of 25.2 ML Ge, resulting in the appearance of huge Ge superdomes in company with many smaller domes. These Ge superdomes are fully strain-relaxed from XTEM observation, leading to the generation of numerous dislocations at the Ge/Si interface that also propagate through the entire QDs. Such an occurrence of Ge superdomes seriously degrades the crystalline quality of thin-film-like QD materials and thus degrades the ZT value.[27] The QD scenario dramatically changes when a thin separating layer of Si is inserted between the alternative, excessive Ge deposition. Fig. 1(b) reveals the absence of superdome in the 2-fold CQD sample even though these CQDs have the same equivalent Ge deposition of 25.2 ML. The total CQD density is much higher than that in Fig. 1(a). Meanwhile, transition pyramids (T-pyramids) become predominant in a higher density over domes does, which is also evidenced by the corresponding SOMs. These results are ascribed to the suppressed surface diffusion of Ge as a consequence of the Si insertion between the Ge sub-dots. The relatively low surface diffusivity of Si effectively slows down the exchange of Ge among the CQDs, thus suppressing the CQD coarsening. We further found that the shape and size distribution of 2-fold CQDs are well tunable by the thickness of the Si inserting layer. Fig. 1(c) clearly shows that uniform dome-shaped CQDs are formed when the inserted Si thickness is reduced to 1 nm. Recently, Hopkins *et al.* reported that an increased physical roughness at the interfaces in QD structures facilitates additional phonon resistive processes beyond the interfacial vibrational mismatch, resulting in a further reduction in κ.[28] Our CQD structures provide a strategy for tuning the Si/CQD/Si interfacial roughness for thin-film-like TE materials.

The formation mechanism of CQDs is revealed via the time-evolutional morphology change of the Ge QDs through selective removal of the Ge-rich parts of dots for different durations. Fig. 2(a) clearly reveals that the etched Ge superdomes initially exhibit roughly circle structures for a minimal Gibbs free energy from a thermodynamic perspective. The

difference in chemical potentials makes released Si from the surrounding Si substrate to intermix with the Ge superdomes, resulting in Si enrichment in the periphery of superdomes. A further etching reveals that a Ge superdome is composed of numerous Ge QDs, a result of QD coarsening [Fig. 2(d)]. On the other hand, the 2-fold CQDs were also etched from their apices initially [Fig. 2(b) and (c)], and further etching produced remarkably different features depending on the inserted Si thickness. The 2-fold CQDs that have a 2-nm-thick inserting layer of Si exhibit a fortress-like feature [Fig. 2(e)], whereas square plateaus are observed for the CQDs with a thinner inserted Si [Fig. 2(f)]. Our previous work discovered that the Ge QDs have a shape transition from dome to truncated pyramid during the initial stages of Si encapsulation.[29] The shape transition tends to achieve an equilibrium morphology that depends on the QD's volume and composition. It is believed that a thinner inserting layer of Si in CQDs is conducive for fully intermixing with the underlying Ge sub-dots to form alloyed pyramids, serving as nucleation seeds for the subsequent Ge sub-dot deposition. Hence, the etching experiment discloses orderly square plateaus under the 2-fold CQDs that have a 1-nm-thick Si inserting layer. For those CQDs with a thicker inserting layer of Si, the excess Si deposited over the already alloyed pyramids may be expelled from the pyramid apex to its sides or corners based on thermodynamic or kinetic considerations,[25,29,30] thus resulting in a fortress-like isocompositional profile [Fig. 2(e)]. These results also suggest that the thickness of the Si inserting layer not only alters the compositional distribution within the CQDs but also changes the strain modulations for upper sub-dot nucleation, thus enabling the manipulation on the shape and size distribution of CQDs.

The 2-fold CQDs also exhibit a distinct coarsening behavior during *in situ* post-growth annealing. As reported previously, post-growth annealing usually causes serious QD coarsening and strong SiGe intermixing.[31,32] This is also confirmed by our systematic AFM characterizations [Fig. 3(a)] on the regular QDs obtained by the deposition of 12.6 ML Ge,

followed by *in situ* post-growth annealing and subsequent selective chemical etching. An apparent reduction in QD density is clearly observed following post-growth annealing. Meanwhile, the as-grown QDs transform from a bimodal distribution that includes both domes and square pyramids to larger domes only. The selective etching further reveals that the annealed Ge QDs exhibit half-moon-like structures, which occupy most volume of the original QDs. This compositional profile is a result of lateral dot motion that is driven by asymmetric surface-mediated alloying during annealing.[18,24] Such a dot migration on the Si surface also enhances the SiGe intermixing in QD coarsening, leading to a high concentration of Si in the annealed QDs. Conversely, the CQD density remains nearly unchanged after annealing, except that some of dome-shaped CQDs become larger, as seen in Fig. 3(b). This is because of the low mobility for the underlying Ge sub-dots in the CQDs (the above-mentioned SiGe-alloyed pyramids) due to the relatively low surface diffusivity of Si. Therefore, only part of Ge in the upper sub-dots is able to migrate from the original CQDs to the new ones. The TEM micrographs in Fig. 4 clearly illustrate this transition; some CQDs grow in size after annealing and others shrink but never disappear. Detailed TEM characterization further shows that the 2-fold CQDs remain dislocation-free after post-growth annealing. These observations suggest that not only the CQDs are highly resistive to QD coarsening during thermal annealing but also the structural parameters of CQDs is tunable by conditions of the post-growth annealing.

To enhance the phonon scattering in nanostructured materials for better TE performance, we attempt to incorporate more sub-dot stacks into the CQDs for the creation of more Ge/Si interfaces and boundary scattering sites. The AFM images in Fig. 5(a)-(c) compare the surface morphology of 2-fold, 3-fold, and 5-fold CQDs, respectively. An increase in the sub-dot stacks of the CQDs makes the CQDs growth in size. Remarkably no superdome is observed in these CQD samples even though 5 times the usual Ge deposition was

incorporated in the 5-fold CQDs. However, some large, irregular-shaped domes that have shallow facets were observed for the 5-fold CQD sample, as indicated by white arrows in Fig. 5(c). This produces non-uniform strain modulations and thus generates defects in the growth of thin-film materials in sufficient thickness. As shown in Fig. 5(d) and (e), the etched features suggest that the inserting layers of Si in the 2-fold and 3-fold CQDs are not pure Si and inhomogeneous in thickness, so that thinner and alloyed regions are not able to protect the underlying sub-dots during etching and thus depressions near the center of a CQD appear. The experimental finding from Fig. 5(d) and (e) also suggests that the inserting layer of Si suffers from a substantial strain filed, leading to Si redistribution on the sub-dots during deposition. On the contrary, only the Ge-rich part of the topmost sub-dots was removed from the 5-fold CQDs [Fig. 5(f)], indicating that the topmost inserting layer of Si in the 5-fold CQDs is relatively homogeneous in thickness and strong enough to prevent the underlying Ge sub-dots from chemical etching. We infer that when incorporating more sub-dot stacks into the CQDs, the growing CQDs conversely disperse the substantial strain field for the subsequent growth. Such a dispersive strain field may disturb the Si or Ge redistribution in the deposition, making the topmost inserting layer of Si more homogeneous in thickness and inducing irregular-shaped 5-fold CQDs seen in Fig. 5(c). Indeed, the structural parameters of 5- or even more-fold CQDs can be further optimized by tuning the thickness of the Si inserting layer as above-discussed.

The XTEM micrographs in Fig. 6(a) and (b) illustrate the thin-film-like regular-QD and CQD materials that are composed of 40-period regular-QD/Si and 3-fold-CQD/Si stacks, respectively. No threading defect, such as dislocation, is observable for these stacks. The higher-magnification micrograph in Fig. 6(b) further reveals a strict vertical alignment of 3-fold-CQD/Si stacks, indicating a substantial and appropriate strain field produced in the thin-film-like CQD material. These results demonstrate the effectiveness of the proposed

CQDs on the production of a thin-film-like CQD material with sufficient thickness, high Ge/Si interface density, and high quality for practical TE applications.

Fig. 7(a) shows the effective $\kappa_{\perp}$ values of the thin-film-like regular-QD, 2-, and 3-fold-CQD systems as a function of temperatures. An interesting finding is that the effective $\kappa_{\perp}$ decreases with an increase in the fold of CQDs. Among these thin-film-like materials, the 3-fold-CQD sample exhibits the lowest $\kappa_{\perp}$ values of 5–7.5 W/m·K over the range of experimental temperatures. At room temperature, its $\kappa_{\perp}$ value is 6.7 W/m·K, which is a factor of approximate 10 and 25 lower than that of bulk Si (~130 W/m·K) and bulk Ge (~60 W/m·K), respectively. Intuitively, this improvement in $\kappa_{\perp}$ is a benefit of enhanced boundary scattering sites from the higher Si/Ge interface density in the CQD samples. Another interesting finding from the temperature dependent $\kappa_{\perp}$(T) characteristics is that the κ_{max} plateau occurred in the mid-temperature regime, at which $\kappa_{\perp}$ reaches its maximum value as a consequence of phonon-phonon scattering and impurity scattering dominant over the temperature-independent boundary scattering.[2,23] In comparison with the $\kappa_{\perp}$ (T) curve of the thin-film-like regular-QD sample, a slight shift of κ_{max} plateau to the lower temperature coupled with a reduced κ_{max} plateau for the thin-film-like 2- and 3-fold-CQD materials in Fig. 7(a) suggests that the local alloying regions near the center of the CQD also play an important role in phonon scattering mechanism. Many previous works have demonstrated that the implantation of dopants into the Si or SiGe thin films induces a reduction in the $\kappa_{\perp}$ as a result of enhanced phonon-impurity scattering.[33,34] We have performed the κ measurement on the B-implanted samples at room temperature, and a 10–45% reduction has been observed for the CQD samples (see Fig. S1). Fig. 7(b) further shows the corresponding σ values of the thin-film-like regular-QD, 2-, and 3-fold-CQD systems as a function of temperatures. The $\sigma(T)$ curves for these thin-film-like CQD materials exhibit typical temperature dependence for the doped

semiconductor in the experimental temperature regime, i.e., σ declines with increasing temperature.[35] Notably σ appears to improve with an increase in the fold of CQDs, a consequence of more Ge incorporation into the multi-fold CQDs.[36]

Currently, we presented the $\kappa_{\perp}$ value and in-plane σ of the thin-film-like CQD materials. The characterization of Seebeck coefficient on the experimental QD structures is ongoing. Many attempts have been made on the investigations of the anisotropy of κ and σ for Si/Ge superlattice structures. Similar anisotropy has been observed for both electrons/holes and phonon transport behaviors.[13,37] For instance, the in-plane κ of the Si/Ge superlattice is 5–6 times higher than the cross-plane one, and the anisotropy of 4.96 is found from the measured cross-plane ($117\ \Omega^{-1}m^{-1}$) and in-plane ($580\ \Omega^{-1}m^{-1}$) σ values.[13] Assuming the Seebeck coefficients for our QD materials being identical, the estimated ZT value for the 3-fold-CQD sample is approximately 1.5 times higher than that of the regular QDs at room temperature. We envisage further scientific exploration of this proposed multi-fold CQD heterostructure for the optimal ZT and the practical TE applications.

4. Conclusions

In summary, the structural parameters of CQDs, such as dot morphology, Si/Ge interface density, and composition distribution, are able to be effectively tailored by the inserting layer of Si thickness, the number of sub-dot stacks, and a post-growth annealing. The formation mechanism for the CQDs is clarified by selective chemical etching experiments. Compared to regular-QD materials, the thin-film-like multifold-CQD materials exhibit both reduced $\kappa_{\perp}$ and enhanced σ, and a 1.5 times higher *ZT* value by calculation, providing a promising building block for practical thermoelectric applications in micro- or nanoelectronics.

ACKNOWLEDGMENTS

The research is supported by National Nano Device Laboratories and National Science Council of Taiwan under Contract No. NSC-100-2221-E-008-016-MY3 and NSC-99-2221-E-008-095-MY3. The authors also thank National Nano Device Laboratories and Center for Nano Science and Technology at National Central University for the facility support.

REFERENCES

1. G. J. Snyder and E. S. Toberer, *Nat. Mater*., 2008, **7**, 105-114.
2. N. Mingo, D. Hauser, N. P. Kobayashi, M. Plissonnier and A. Shakouri, *Nano Lett*., 2009, **9**, 711-715.
3. K. Biswas, J. He, I. D. Blum, C. I. Wu, T. P. Hogan, D. N. Seidman, V. P. Dravid and M. G. Kanatzidis, *Nature*, 2012, **489**, 414-418.
4. C. L. Hsin, M. Wingert, C. W. Huang, H. Guo, T. J. Shih, J. Suh, K. Wang, J. Wu, W. W. Wu and R. Chen, *Nanoscale*, 2013, **5**, 4669-4672.
5. D. Yang, C. Lu, H. Yin and I. P. Herman, *Nanoscale*, 2013, **5**, 7290-7296.
6. P. E. Hopkins, C. M. Reinke, M. F. Su, R. H. Olsson III, E. A. Shaner, Z. C. Leseman, J. R. Serrano, L. M. Phinney and I. El-Kady, *Nano Lett*., 2011, **11**, 107-112.
7. J. Fu, S. Song, X. Zhang, F. Cao, L. Zhou, X. Li and H. Zhang, *CrystEngComm*, 2012, **14**, 2159-2165.
8. A. I. Hochbaum, R. Chen, R. D. Delgado, W. Liang, E. C. Granett, M. Najarian, A. Majumdar and P. Yang, *Nature*, 2008, **451**, 163-167.
9. L. Shi, D. Yao, G. Zhang and B. Li, *Appl. Phys. Lett*., 2010, **96**, 173108.
10. M. T. Hung, C. C. Wang, J. C. Hsu, J. Y. Chiou, S. W. Lee, T. M. Hsu and P. W. Li, *Appl. Phys. Lett*., 2012, **101**, 251913.
11. A. S. Henry and G. Chen, *J. Comput. Theor. Nanosci*., 2008, **5**, 141-152.
12. K. Hippalgaonkar, B. Huang, R. Chen, K. Sawyer, P. Ercius and A. Majumdar, *Nano Lett*., 2010, **10**, 4341-4348.
13. B. Yang, W. L. Liu, J. L. Liu, K. L. Wang, and G. Chen, *Appl. Phys. Lett.*, 2002, **81**, 3588-3590.
14. J. L. Liu, A. Khitun, K. L. Wang, T. Borca-Tasciuc, W. L. Liu, G. Chen and D. P. Yu, *J. Cryst. Growth*, 2001, **227-228**, 1111-1115.
15. M. L. Lee and R. Venkatasubramanian, *Appl. Phys. Lett*., 2008, **92**, 053112.
16. J. L. Liu, A. Khitun, K. L. Wang, W. L. Liu, G. Chen, Q. H. Xie and S. G. Thomas, *Phys. Rev. B*, 2003, **67**, 165333.
17. G. Pernot, M. Stoffel, I. Savic, F. Pezzoli and P. Chen, *Nat. Mater*., 2010, **9**, 491-495.

18. U. Denker, A. Rastelli, M. Stoffel, J. Tersoff, G. Katsaros, G. Costantini, K. Kern, N. Y. Jin-Phillipp, D. E. Jesson and O. G. Schmidt, *Phys. Rev. Lett*., 2005, **94**, 216103.

19. A. Rastelli, M. Stoffel, A. Malachias, T. Merdzhanova, G. Katsaros, K. Kern, T. H. Metzger and O. G. Schmidt, *Nano Lett*., 2008, **8**, 1404-1409.

20. E. Mateeva, P. Sutter, J. C. Bean and M. G. Lagally, *Appl. Phys. Lett*., 1997, **71**, 3233-3235.

21. S. W. Lee, H. T. Chang, C. H. Lee, S. L. Cheng and C. W. Liu, *Thin Solid Films*, 2010, **518**, S196-S199.

22. Y. Ma, S. Huang, C. Zeng, T. Zhou, Z. Zhong, T. Zhou, Y. Fan, X. Yang, J. Xia and Z. Jiang, *Nanoscale*, 2013, DOI: 10.1039/C3NR04114J.

23. H. T. Chang, C. C. Wang, J. C. Hsu, M. T. Hung, P. W. Li and S. W. Lee, *Appl. Phys. Lett*., 2013, **102**, 101902.

24. G. Katsaros, A. Rastelli, M. Stoffel, G. Isella, H. von K¨anel, A. M. Bittner, J. Tersoff, U. Denker, O. G. Schmidt, G. Costantini, and K. Kern, *Surf. Sci.*, 2006, **600**, 2608-2613.

25. F. H. Li, Y. L. Fan, X. J. Yang, Z. M. Jiang, Y. Q. Wu and J. Zou, *Appl. Phys. Lett*., 2006, **89,** 103108.

26. J. Cui, Y. Lv, X. J. Yang, Y. L. Fan, Z. Zhong and Z. M. Jiang, *Nanotechnology*, 2011, **22**, 125601.

27. J. R. Watling and D. J. Paul, *J. Appl. Phys. Lett.*, 2011, 110, 114508.

28. P. E. Hopkins, J. C. Duda, C. W. Petz, and J. A. Floro, *Phys. Rev. B*, 2011, **84**, 035438.

29. S. W. Lee, L. J. Chen, P. S. Chen, M.-J. Tsai, C. W. Liu, T. Y. Chien, and C. T. Chia, *Appl. Phys. Lett.*, 2003, **83**, 5283-5285.

30. U. Denker, M. Stoffel, and O. G. Schmidt, *Phys. Rev. Lett*., 2003, **90**, 196102.

31. J. A. Floro, M. B. Sinclair, E. Chason, L. B. Freund, R. D. Twesten, R. Q. Hwang and G. A. Lucadamo, *Phys. Rev. Lett.*, 2000, **84**, 701-704.

32. T. I. Kamins, G. Medeiros-Ribeiro, D. A. A. Ohlberg, and R. S. Williams, *J. Appl. Phys.*, 1999, **85**, 1159-1171.

33. C. N. Liao, C. Chen, and K. N. Tu, *J. Appl. Phys.*, 1999, **86**, 3204-3208.

34. M. Takashiri, T. Borca-Tasciuc, A. Jacquot, K. Miyazaki, and G. Chen, *J. Appl. Phys.*,

2006, **100**, 054315.

35. M. J. Katz, *Phys. Rev.*, 1965, **140**, A1323-A1344.

36. S. C. Hsu, C. L. Hsin, C. W. Huang, S. Y. Yu, C. W. Wang, C. M. Lu, K. C. Lu, and W. W. Wu, *CrystEngComm*, 2012, **14**, 4570-4574.

37. G. Chen, *Phys. Rev. B*, 1998, **57**, 14958-14973.

FIGURE CAPTIONS

Figure 1 AFM (1μm × 1μm) and XTEM micrographs of as-grown (a) 25.2-ML Ge QDs, (b) 2-fold, and (c) 3-fold CQDs, in which transition pyramids, pyramids, domes, and superdomes are denoted by "T", "P", "D", and "SD", respectively. The insets of AFM images also show the corresponding SOMs with different symbols marking different facets.

Figure 2 AFM images (1μm × 1μm) showing the 25.2-ML Ge QDs, 2-fold, and 3-fold CQDs after selective chemical etching for (a)-(c) 1 h and (d)-(f) 5 h, respectively. Transition pyramids, pyramids, domes, and superdomes follow the abbreviations shown in Fig. 1.

Figure 3 AFM images (1μm × 1μm) illustrating the transition of as-grown (a) 12.6-ML Ge QDs and (b) 2-fold CQDs followed by *in situ* post-growth annealing for 1 h and subsequent selective chemical etching for 5 h. The insets of AFM images show the corresponding SOMs.

Figure 4 XTEM micrographs of single-layer 2-fold CQDs (a) before and (b) after annealing for 1 h. Higher-magnification XTEM micrographs in the bottom further shows the representative CQDs taken from (b).

Figure 5 AFM (1μm × 1μm) images of single-layer (a) 2-, (b) 3-, and (c) 5-fold CQDs and (d)-(f) followed by selective etching for 5 h. The insets of AFM images also show the corresponding SOMs.

Figure 6 XTEM micrographs of thin-film-like (a) regular-QD and (b) CQD materials consisting of 40-period regular-QD/Si and 3-fold-CQD/Si stacks, respectively. The right column of (b) also shows a higher-magnification image for a selected region near the topmost CQD/Si stack.

Figure 7 (a) Effective thermal conductivities $\kappa_{\perp}$ and (b) electrical conductivities σ as a

function of experimental temperatures for the thin-film-like regular-QD and CQD materials. The schematic diagrams for our κ and σ measurement devices are also shown in the figure.

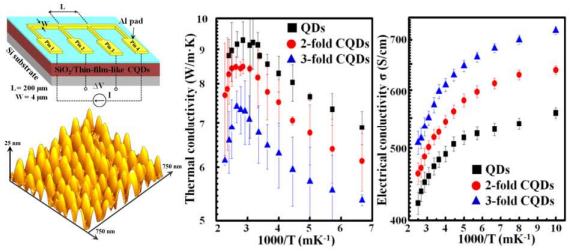

Designer multifold-CQD materials exhibit both a reduced thermal conductivity and an enhanced electrical conductivity, and a higher *ZT* by calculation.

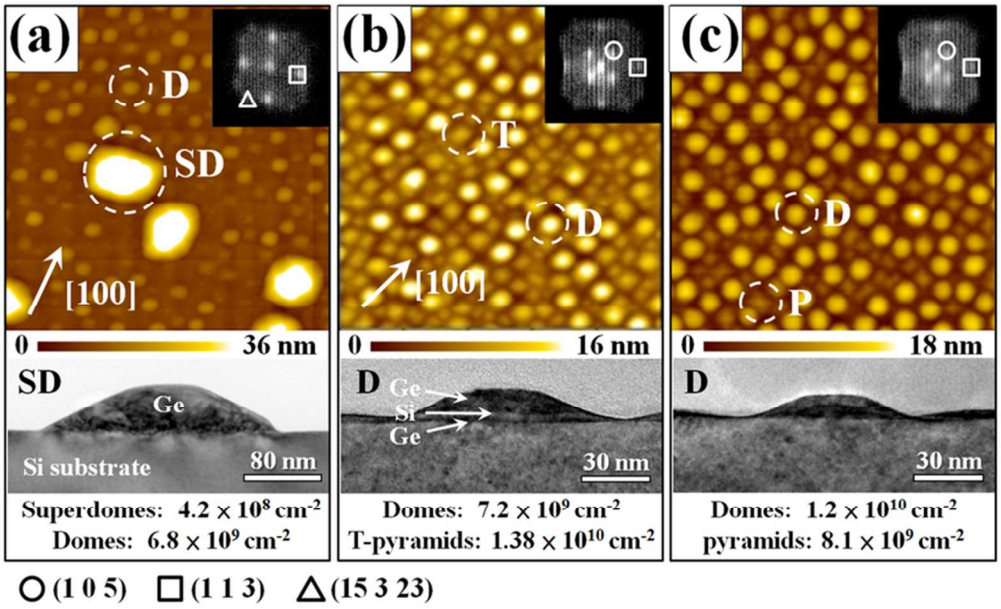

73x44mm (300 x 300 DPI)

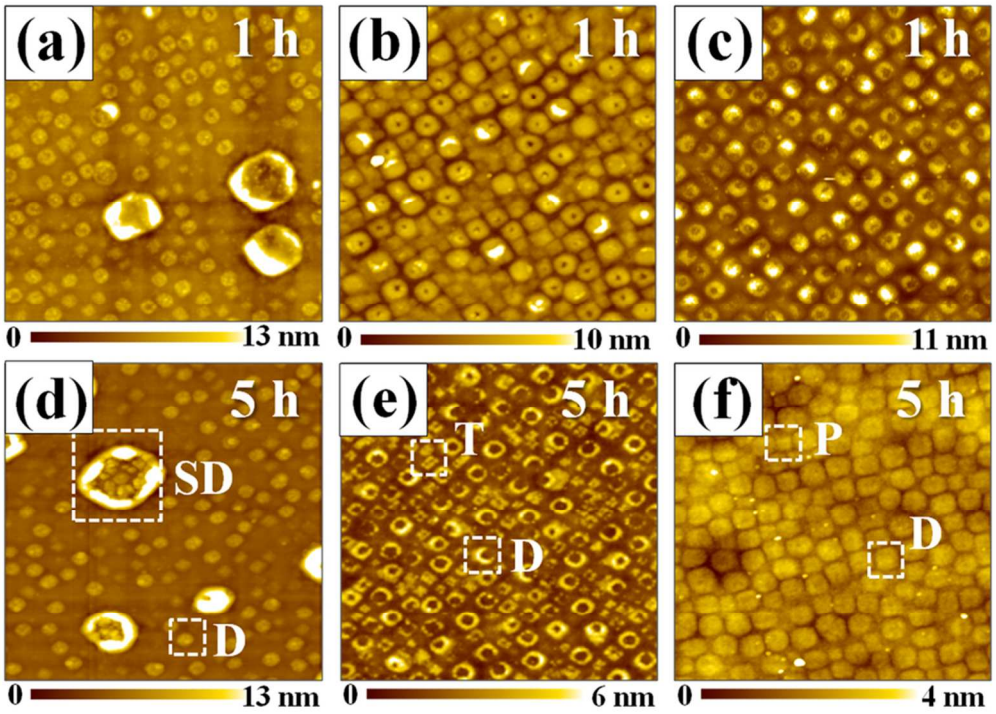

86x61mm (300 x 300 DPI)

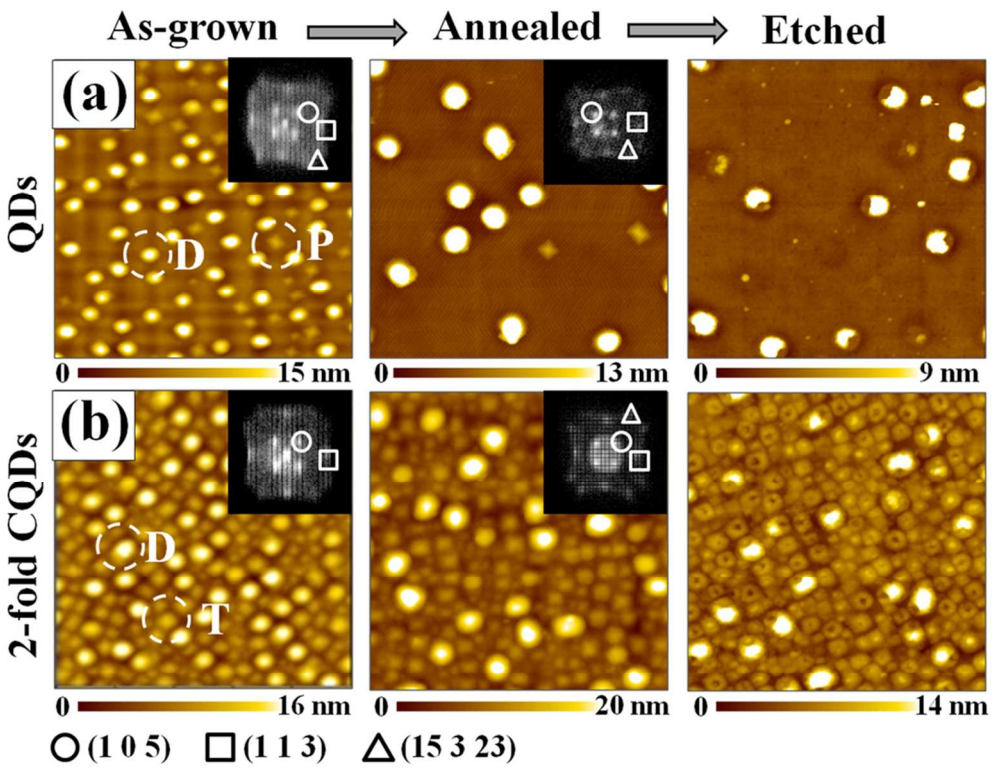

91x69mm (300 x 300 DPI)

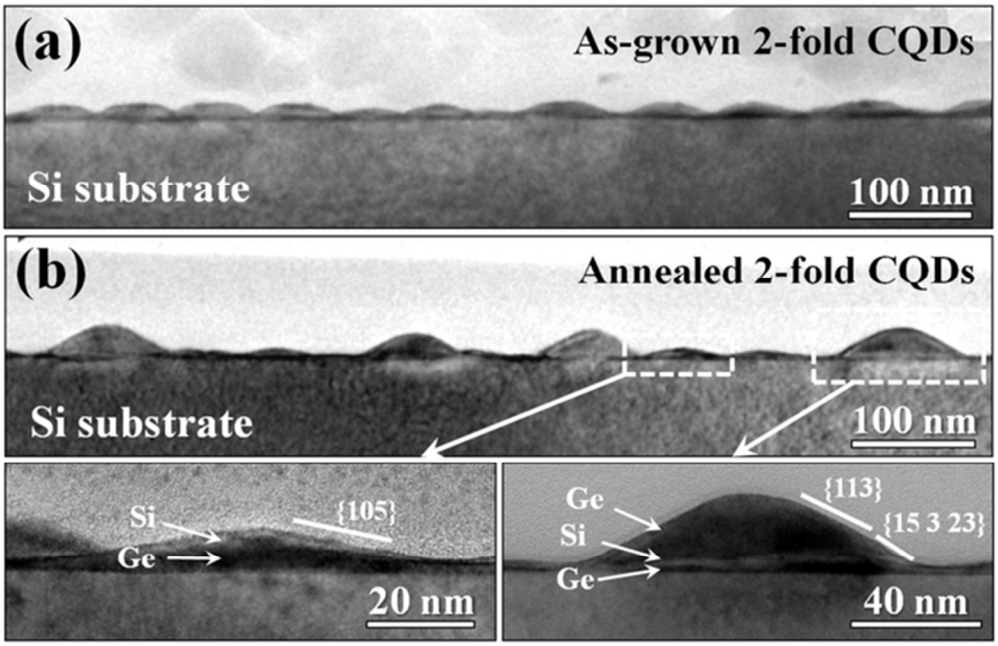

58x38mm (300 x 300 DPI)

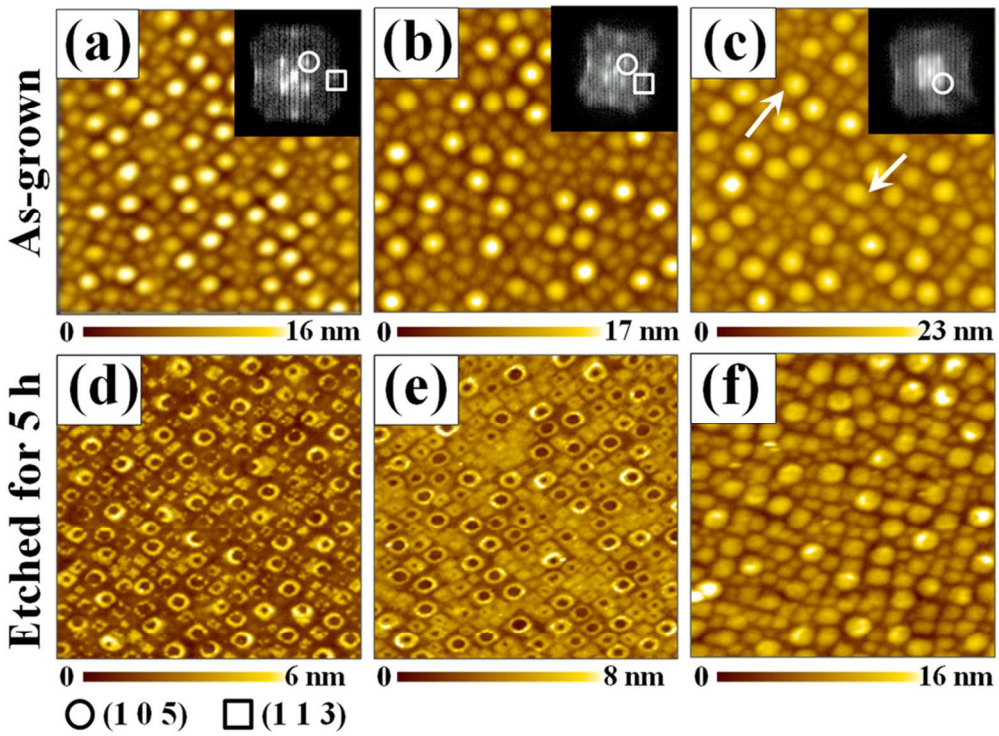

87x64mm (300 x 300 DPI)

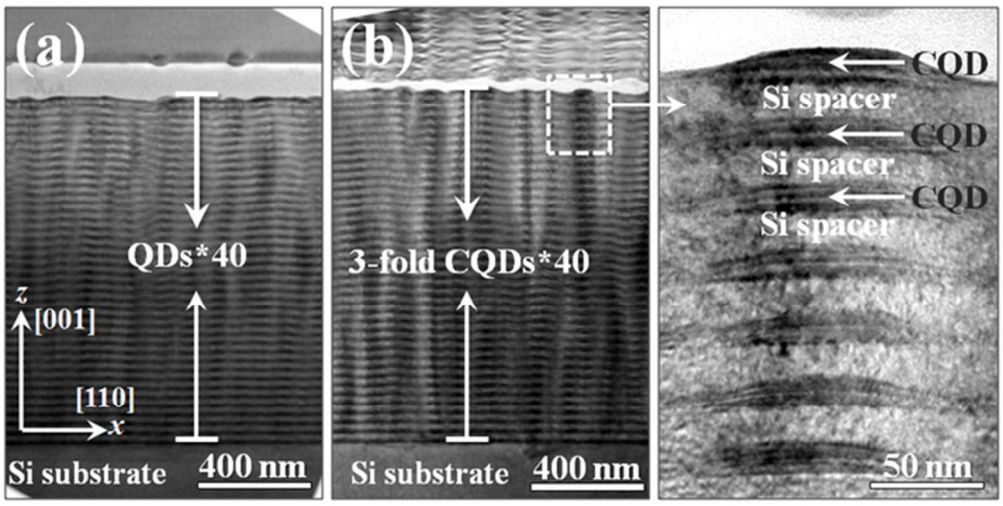

60x30mm (300 x 300 DPI)

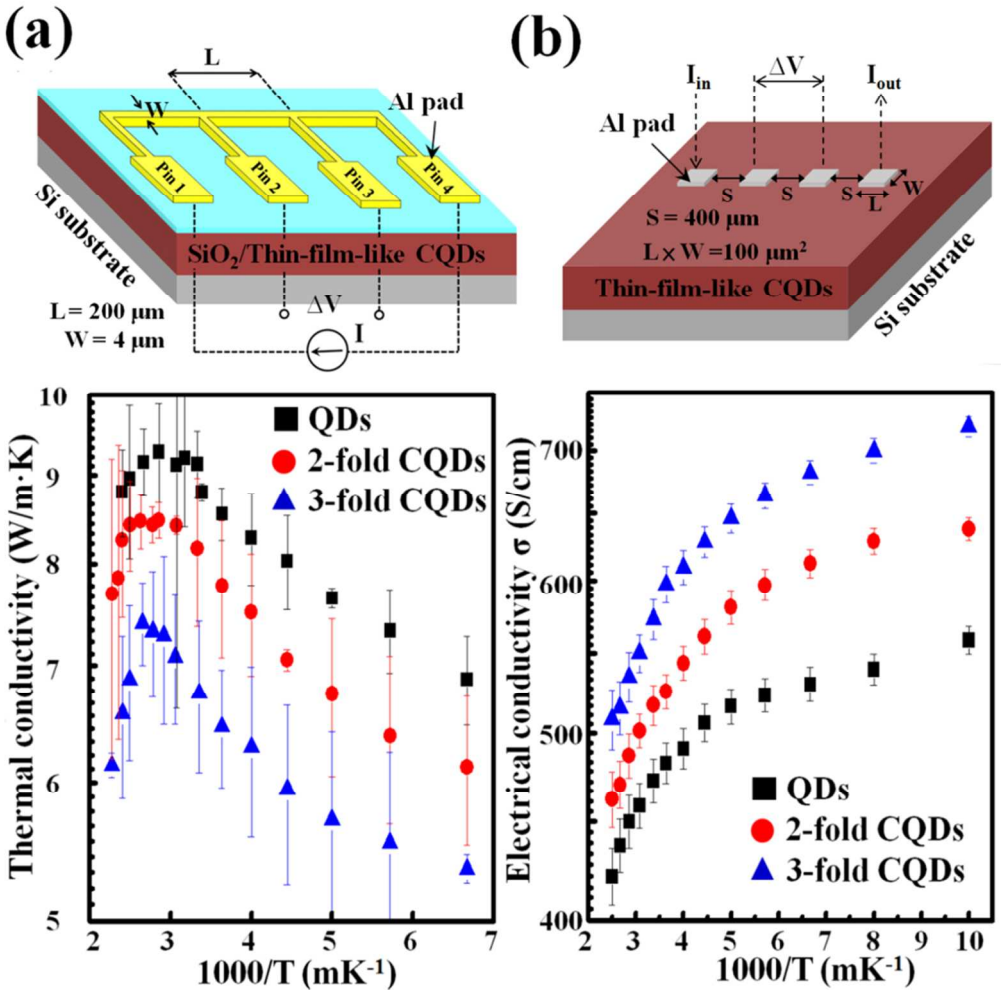

119x118mm (300 x 300 DPI)